Different mechanism of response of asymmetric lone pair electrons around ns² cations to birefringence and second harmonic generation

Cite as: J. Appl. Phys. **128**, 113104 (2020); https://doi.org/10.1063/5.0022878 Submitted: 24 July 2020 . Accepted: 03 September 2020 . Published Online: 21 September 2020

Xuerui Shi, D Qun Jing, Zhaohui Chen, Ming-Hsien Lee, Haiming Duan, and Hanqin Ding







ARTICLES YOU MAY BE INTERESTED IN

Nonlinear magnetoelectric effects in Y-type hexaferrite microwave resonators Journal of Applied Physics 128, 113905 (2020); https://doi.org/10.1063/5.0021593

Chemical substitution induced half-metallicity in $CrMnSb_{(1-X)}P_X$ Journal of Applied Physics 128, 113906 (2020); https://doi.org/10.1063/5.0021467

Highly efficient meta-radiators with circular polarization

Journal of Applied Physics 128, 114503 (2020); https://doi.org/10.1063/5.0011652



Your Qubits. Measured.

Meet the next generation of quantum analyzers

- Readout for up to 64 qubits
 Operation at up to 8.5 GHz
 - Operation at up to 8.5 GHz, mixer-calibration-free

 Signal optimization with minimal latency





Different mechanism of response of asymmetric lone pair electrons around ns² cations to birefringence and second harmonic generation

Cite as: J. Appl. Phys. **128**, 113104 (2020); doi: 10.1063/5.0022878 Submitted: 24 July 2020 · Accepted: 3 September 2020 · Published Online: 21 September 2020







Xuerui Shi, Qun Jing, 1,a) 📵 Zhaohui Chen, Ming-Hsien Lee, Haiming Duan, and Hanqin Ding 1,a)

AFFILIATIONS

¹School of Physical Science and Technology and School of Chemical Engineering and Technology, Xinjiang University, 666 Shengli Road, Urumqi 830046, China

ABSTRACT

The $6s^2$ lone-pair electrons (Pb²⁺, Bi³⁺) and $5s^2$ lone-pair electrons (Sn²⁺, Sb³⁺) show different responses to birefringence than they do to second harmonic generation (SHG). In the current work, different mechanisms of birefringence and SHG responses induced by Pb²⁺/Sn²⁺ cations were investigated using the first-principles method on AB₂O₃F₂ (A = Ba, Sn, Pb). The obtained birefringence and SHG coefficients were in good agreement with the experimental values. The anisotropic lone-pair electron distribution was found at the states near the Fermi level containing cation sp-oxygen p states. Our analyses showed the birefringences of the AB₂O₃F₂ (A = Ba, Sn, Pb) compounds to be directly affected by the anisotropic lone-pair electron distribution, however, the SHG responses of these three compounds have a more complicated relationship with the hybrid cation-oxygen states. The expanded hybrid cation-oxygen states including the lone-pair states were concluded to endow the PbB₂O₃F₂ compound with a stronger SHG response than those displayed by the other compounds.

Published under license by AIP Publishing. https://doi.org/10.1063/5.0022878

I. INTRODUCTION

Due to the demand for novel nonlinear optical (NLO) materials with strong second harmonic generation (SHG) responses and suitable levels of birefringence, there has been a steady impetus to design and synthesize new kinds of NLO compounds. ^{1–7} In the past few decades, borates have attracted a lot of attention, not only because they come in so many different structural variations and include favorable structural units with large nonlinear susceptibilities, but also because they have been used to obtain a good supply of NLO materials with excellent optical properties, ^{8–17} with examples including KBe₂(BO₃)F₂(KBBF), ^{18,19} Sr₂Be₂B₂O₇(SBBO), ²⁰ LiB₃O₅(LBO), ²¹ CsB₃O₅ (CBO), ²² etc.

As a general strategy, replacing alkali metal/alkaline earth metal cations with lone-pair electron cations has been thought to be beneficial for achieving enhanced birefringence and/or SHG response. Enhanced SHG responses have been found, for example, in $Pb_2B_5O_9X$ (X = Cl, Br, I) $^{27-29}$ $Pb_2BO_3X(X = Cl, Br, I),^{30-32}$ $Pb_2Ba_3(BO_3)_3X(X = Cl, Br),^{33,34}$ α -BiB₃O₆ (BiBO), 35,36 Cd₄BiO(BO₃)₃, 37 and so on. Previous

reports demonstrated that introducing lone-pair electron cations can simultaneously yield an enhanced SHG response and birefringence.³⁸ Along with the increasing amount of new NLO compounds, the different responses to birefringence and SHG coefficients induced by ns² lone-pair electrons are also available. For example, birefringence values of a material made out of Sn₂B₅O₉Cl have been measured to be as high as 0.168 at 546 nm, but the SHG response of this material is only 0.5 × KDP.³⁹ Recently, two isomorphic compounds containing lonepairs electrons, namely, PbB₂O₃F₂ and SnB₂O₃F₂, were synthesized.⁴⁰ Interestingly, they showed considerably different birefringence values and SHG responses. PbB2O3F2 achieved a favorable SHG response of $13 \times \text{KDP}$, 3.25 times that of $\text{SnB}_2\text{O}_3\text{F}_2$ (4 × KDP), but the birefringence of SnB₂O₃F₂ (0.130 at 1064 nm) was 7.6 times that of PbB₂O₃F₂ (0.017 at 1064 nm). These results have led to several unresolved questions. Do these compounds display anisotropic ns² lone-pair electron distributions? What is the origin of their enhanced/reduced birefringence levels and SHG responses? What is the role played by the ns² electrons in their levels of anisotropic birefringence and SHG response?

²Department of Physics, Tamkang University, New Taipei City 25137, Taiwan

^{a)}Authors to whom correspondence should be addressed: <code>qunjing@xju.edu.cn</code> and <code>dinghg@xju.edu.cn</code>

We set out to answer these questions in the current work. Specifically, the electronic structures and optical properties of a series of $AB_2O_3F_2$ (A=Ba, Sn, Pb) compounds were investigated using the first-principles method. An anisotropic lone-pair electron distribution was confirmed according to the projected density of states, the projected band structures, the electron localization function (ELF), and the states near the Fermi level. The atomic and group contributions to birefringence and SHG response were further investigated using the real-space atom-cutting method and the band-resolved SHG method. The results showed the anisotropic lone-pair electron distribution close to the Fermi level to be the main contributor to the birefringence, and the expanded hybrid cation sp-oxygen p states play a key role in determining the enhanced SHG response.

II. NUMERICAL CALCULATION DETAILS

To further elaborate the electronic structures and optical properties of the $AB_2O_3F_2$ (A = Ba, Sn, Pb) compounds, first-principles calculations were performed on them using the CASTEP package. 41,42 Norm-conserving pseudopotentials were chosen, 43,44 and the valence electrons were set as $B:2s^22p^1,\ O:2s^22p^4,\ F:3s^23p^5,\ Sn:5s^25p^2,\ Pb:5s^25p^65d^{10}6s^26p^2,\ and\ Ba:5s^25p^66s^2.$ The Perdew–Burke–Ernzerhof (PBE) functional under the generalized gradient approximation (GGA) 45,46 with a high kinetic energy cutoff of 940 eV was adopted and Monkhorst–Pack k point meshes with $6\times6\times3(BaB_2O_3F_2),\ 6\times6\times6(SnB_2O_3F_2),\ and\ 6\times6\times6(PbB_2O_3F_2)$ points in the Brillouin zone of the unit cell were used.

Based on the electronic structures obtained using CASTEP, the refractive indices and the birefringence values were further calculated using the program OptaDOS. The SHG tensors of $AB_2O_3F_2$ (A = Ba, Sn, Pb) were further investigated using the method described in Refs. 49 and 50.

III. RESULTS AND DISCUSSION

A. The lone-pair electron distribution

Based on the above calculations, the band structures of $AB_2O_3F_2$ (A=Ba, Sn, Pb) along the high-symmetry points of the first Brillouin zone were obtained and are shown in Fig. 1. As shown in this figure, $BaB_2O_3F_2$ was determined from these calculations to be an indirect bandgap compound with a bandgap of 6.67 eV and to have the valence band maximum (VBM) and the conduction band minimum (CBM) located at G and Y, respectively. $SnB_2O_3F_2$ and $PbB_2O_3F_2$ were calculated to have direct bandgaps of, respectively, 4.02 and 5.15 eV, with their VBMs and CBMs located at M. The obtained GGA-PBE bandgaps were smaller than the experimental values. The underestimation of the bandgap in the GGA-PBE functional has been related to the discontinuity of the exchange-correlation energy functional. 51,52

For comparison, the band structures were also calculated using the HSE06 functional $^{53-55}$ implemented in the program PWMAT 56,57 with $6\times6\times3(BaB_2O_3F_2),~6\times6\times6(SnB_2O_3F_2),$ and $6\times6\times6(PbB_2O_3F_2)$ Monkhorst–Pack K-points and an energy cutoff of 816 eV. As shown in Table I, using HSE06 yielded bandgaps of 7.55 eV $(BaB_2O_3F_2),~5.66$ eV $(PbB_2O_3F_2),~and~5.00$ eV $(SnB_2O_3F_2)$. The HSE bandgaps of $SnB_2O_3F_2$ and $SnB_2O_3F_2$ were

found to be comparable to the experimental values. Note that the DUV absorption edge of $BaB_2O_3F_2$ has been described by Huang *et al.* to be below $180\,\mathrm{nm}$, 58 and the bandgaps of some different phases of $BaB_2O_3F_2$ have been pointed out by Zhang *et al.* to be about $8.12-9.0\,\mathrm{eV}$. Hence, the authors believe the obtained HSE bandgap of $BaB_2O_3F_2$ is rational.

The projected densities of states (PDOSs) of these compounds were also obtained (Fig. 1 and S1). As shown in Fig. 1, the cation-sp, O-p, F-p, and B-sp states were found at the top of the valence band and the bottom of the conduction band of each of these compounds. Our main purpose in the work described in this article was to investigate the role played by the lone-pair electrons in the birefringence and SHG response and hence we paid more attention to the states near the Fermi level and the cation sp -O p hybrid orbitals. As shown in Fig. 1, the hybrid cation-oxygen states were found at the energy levels ranging from -10 eV (BaB₂O₃F₂), $-8.6 \,\mathrm{eV}$ (PbB₂O₃F₂), and $-10.3 \,\mathrm{eV}$ (SnB₂O₃F₂) to the Fermi level. Interestingly, at region I in the valence band from -1 eV to the Fermi level, different electronic state features were calculated for these compounds: mainly, O-p states were calculated in this region for BaB2O3F2, implying its states near the Fermi level to be nonbonding states of oxygen atoms; in contrast, Pb-sp states hybridized with O-p states were observed here for PbB₂O₃F₂, and would represent lone-pair electron distributions according to the revised model of lone-pair electrons; 30,59 similar to the case for PbB₂O₃F₂, an Sn-sp state hybridized with O-p states was also found near the Fermi level for SnB₂O₃F₂, indicating that these states may be the lone-pair states of Sn²⁺ cation. The states near the Fermi levels of SnB₂O₃F₂ and PbB₂O₃F₂ did nevertheless show a couple of different features: only one sharp peak for $SnB_2O_3F_2$, but two split peaks for $PbB_2O_3F_2$ and the Sn^{2+} peak being larger (1.06) than the Pb^{2+} peaks (0.18) according to integral calculation results.

The states near the Fermi level were further confirmed using the projected band structures (shown in Fig. 2 and Fig. S2 in the supplementary material). In Fig. 2, only the O-p orbitals appeared near the Fermi level of BaB₂O₃F₂, indicating the O-p orbitals to be the main contributors to the BaB₂O₃F₂. However, for SnB₂O₃F₂ and PbB₂O₃F₂, not only O-p orbitals but also F-s and Sn-sp/Pb-sp orbitals were calculated to be present near the Fermi level. Furthermore, compared with the case for PbB₂O₃F₂, more cation-sp states hybridized with O-p states were found at the Fermi level of SnB₂O₃F₂, implying the presence of more lone-pair electrons in SnB₂O₃F₂.

To further characterize the lone-pair electron distributions around the Sn and Pb atoms, the orbitals near their Fermi levels and their electron localization functions (ELFs) were also investigated (shown in Fig. 3 and Fig. S3 in the supplementary material). As shown in Fig. S3 in the supplementary material, lobe-shaped distributions of electrons around Pb atoms were found at four different states (energy levels of -1.54, -0.81, -0.56, and $0\,\text{eV}$ below the Fermi level), while there was only one state in which a lobe-shaped electron distribution around Sn was found. To better compare and display the characteristics of the lone-pair electrons, a superposition of the lone-pair electrons Pb²⁺ with an energy range from 0 to $-1.54\,\text{eV}$ was made, as shown in Fig. 3(b). Note the completely different isosurface values of these two compounds, i.e., isosurface values of 0.1 and 0.22 for PbB₂O₃F₂ and SnB₂O₃F₂, respectively. That is to say, the distribution of lone-pair electrons

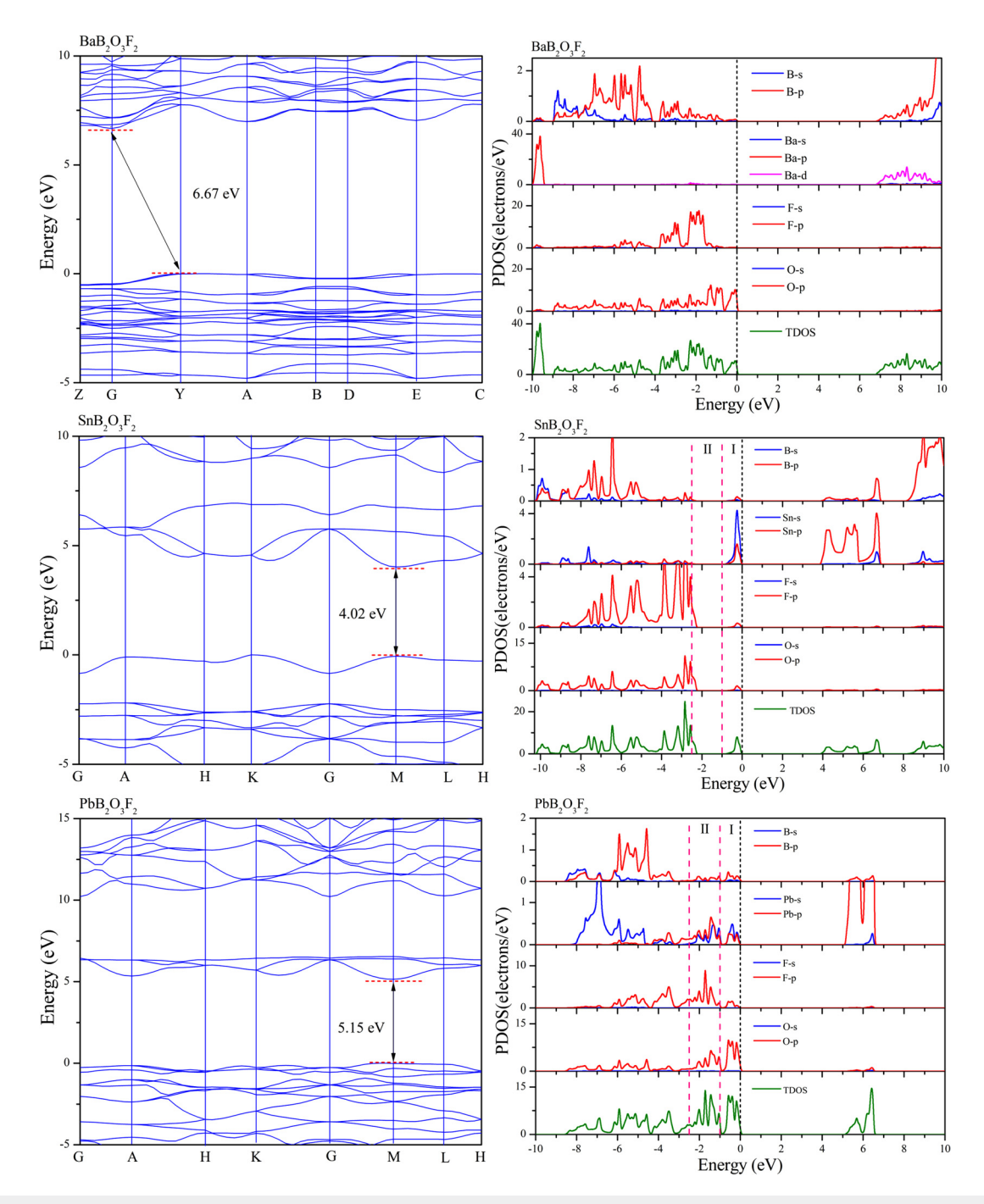


FIG. 1. Band structures and the projected densities of states (PDOSs) of AB₂O₃F₂ (A = Sn, Pb, Ba) determined using CASTEP.

for Sn was calculated to be much obvious than that for Pb. This relationship was also derived from the electron localization function (ELF) analyses, shown in Figs. 3(c) and 3(d). Here, crescent-shaped ELFs were observed around the Sn and Pb atoms, indicative of

asymmetric lone-pair electron distributions around these atoms. Such asymmetric lone-pair electron distributions could lead to enhanced birefringence and other optical properties (described below).

TABLE I. Bandgap values determined using various functionals.

	SnB ₂ O ₃ F ₂	PbB ₂ O ₃ F ₂	BaB ₂ O ₃ F ₂		
$\begin{array}{c} E_g^{HSE06} \text{ (eV)} \\ E_g^{exp} \text{ (eV)} \\ E_g^{PBE} \text{ (eV)} \end{array}$	5.00	5.66	7.55		
$E_{g_{nn}}^{chp}(eV)$	4.96	5.64	•••		
E_{g}^{PBE} (eV)	4.02	5.15	6.67		

B. Refractive indices and birefringence values

Using the method described above, the refractive indices and birefringence values of $AB_2O_3F_2$ (A = Ba, Sn, Pb) were further calculated using the program OptaDOS. The obtained refractive indices and birefringence values are plotted in Fig. 4 and listed in Table II. At a wavelength of 1064 nm, for example, a higher birefringence value was obtained for SnB2O3F2 (0.130) than for $PbB_2O_3F_2$ (0.017) and for $BaB_2O_3F_2$ (0.014).

To better understand the contributions of the atoms and anionic groups to the total birefringence, a real-space atom-cutting method was also used.⁴⁷ The cutting radii of Ba, Sn, Pb, B, O, and F were set to 1.5, 1.2, 1.4, 0.8, 1.1, and 1.2 Å, respectively. The obtained contributions of various ions and anionic groups are shown in Table II. Regarding BaB2O3F2, the anionic group BOF and Ba contributed nearly equally and in each case very little to the total birefringence. The contributions of the BOF groups in the

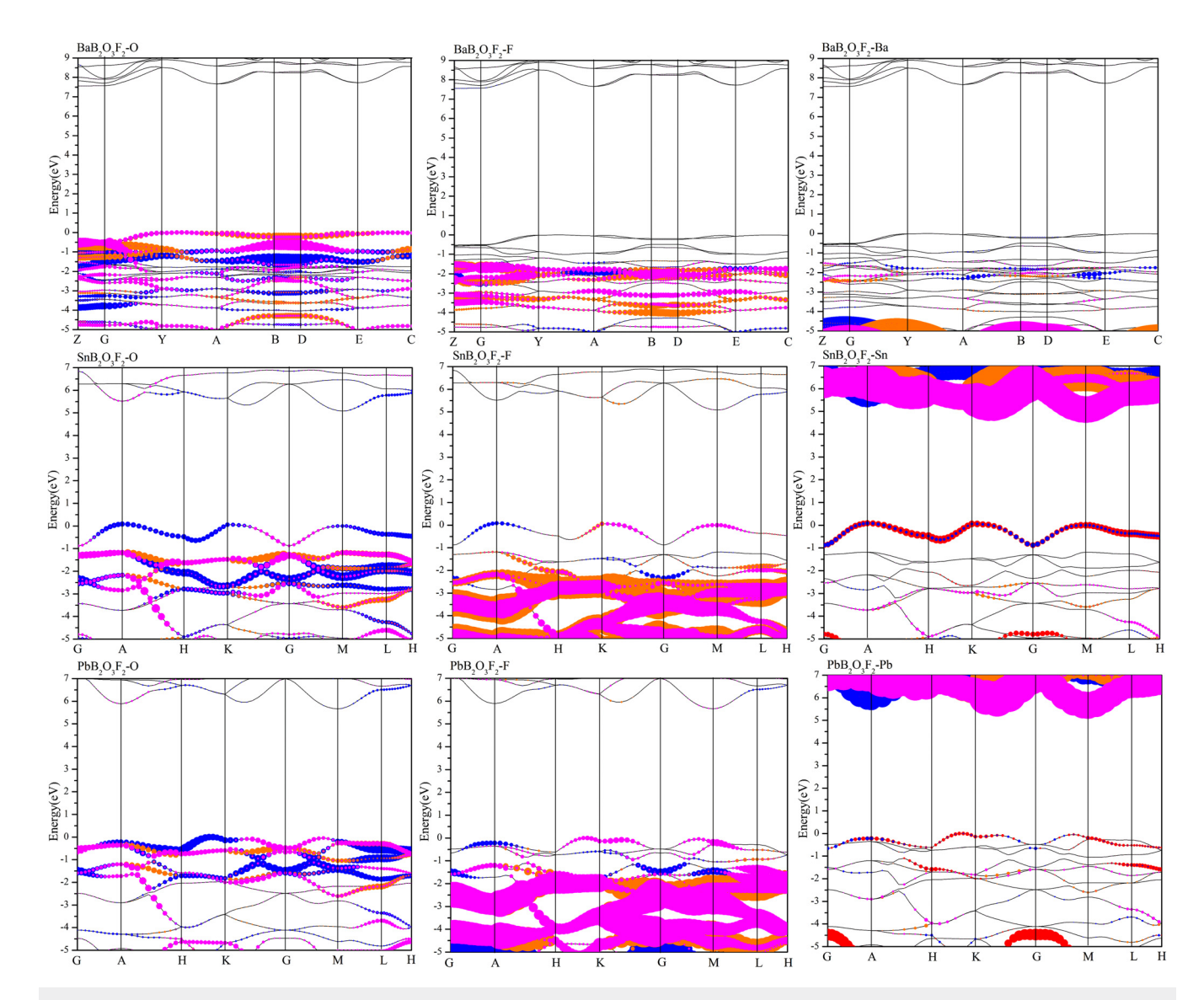


FIG. 2. The projected band structures of AB₂O₃F₂ (A = Ba, Sn, Pb) calculated using the HSE06 functional implemented in PWMAT. The red, orange, pink, and blue points represent the s, p_x , p_y , and p_z states, respectively.

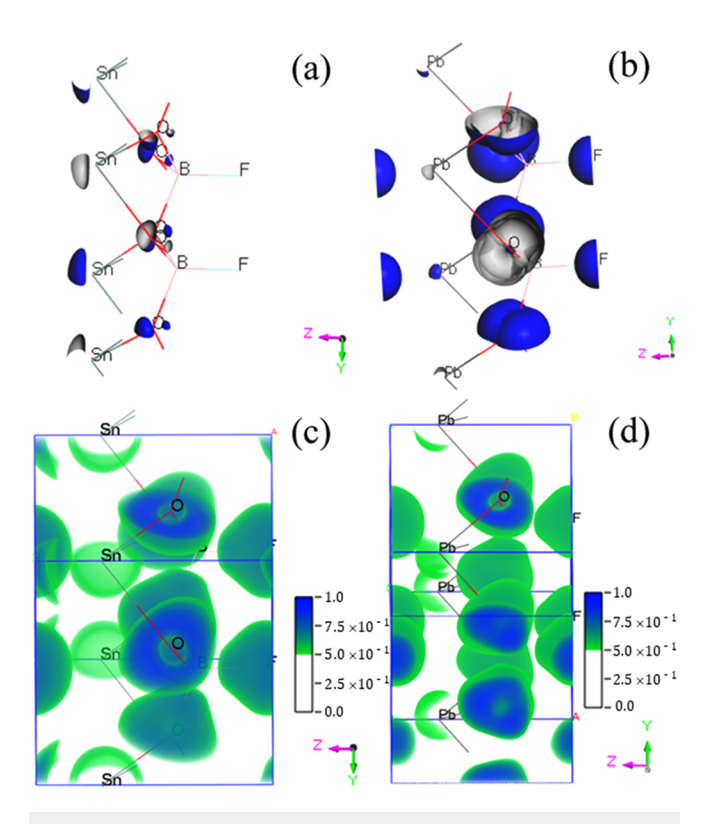


FIG. 3. (a) and (b) Distributions of lone-pair electrons and (c) and (d) electron localization functions (ELFs) around [(a) and (c)] Sn and [(b) and (d)] Pb atoms of the examined compounds.

 $SnB_2O_3F_2$ and $PbB_2O_3F_2$ compounds were indicated to be almost negligible. The main contribution to the birefringence was indicated using the atom-cutting method to derive from the SnO/PbO and PbF groups. At a wavelength of $1064\,\mathrm{nm}$, a much stronger birefringence was indicated for the SnO group (0.177) than for the PbO group (0.017). Note the larger distribution of lone pair electrons around the Sn^{2+} cation than around the Pb^{2+} cation (shown in Fig. 3), and the 5.9-fold greater integral value of the peak in region I of $SnB_2O_3F_2$ (1.06) than of that of $PbB_2O_3F_2$ (0.18). Hence, we believe the lone-pair electrons shown in region I (near the Fermi level) to be the main contributors to the enhancement of birefringence of $SnB_2O_3F_2$ in comparison with those of $PbB_2O_3F_2$ and $BaB_2O_3F_2$.

C. SHG responses

The SHG tensors and evaluated effective SHG coefficients of $AB_2O_3F_2$ (A = Ba, Sn, Pb) were also obtained (shown in Table III along with the experimental values). The effective SHG coefficient was evaluated using the method described in Refs. 60–62 (with more details provided in the supplementary material). The obtained maximum SHG tensors of $PbB_2O_3F_2$ and $SnB_2O_3F_2$ were 4.922 (12.6 × KDP) and 0.962 pm / V (2.5 × KDP), respectively.

The obtained effective SHG responses of $PbB_2O_3F_2$ and $SnB_2O_3F_2$ were 13.0 and 2.2 times that of KDP. As for the experimental values, the obtained effective SHG coefficients and maximum values of the SHG tensor of $PbB_2O_3F_2$ were found to be much larger than those of $SnB_2O_3F_2$.

The atomic contribution to the SHG response was also investigated using the real-space atom-cutting method (with the result shown in Table IV). During the calculation, the scissors were set as the difference between the HSE06-gap and GGA-PBE gap. As shown in Table IV, for the $\rm SnB_2O_3F_2$ and $\rm PbB_2O_3F_2$ compounds, the main contributions were indicated to derive from the SnO/PbO and PbF groups, with a nearly negligible contribution from the BOF group. Furthermore, the contribution from the PbO groups was indicated to be much greater than that from SnO groups, resulting in the stronger SHG response displayed by PbB₂O₃F₂ than by SnB₂O₃F₂. Considering the above-described larger distribution of lone-pair electrons around Sn²⁺ cations than around Pb²⁺ cations, it was curious to us how the PbO groups (and hence PbB₂O₃F₂ compound) could display a much stronger SHG response than the SnO groups (and hence the SnB₂O₃F₂ compound).

To achieve a deep understanding of the different response mechanisms for SHG and birefringence in SnB2O3F2 and PbB₂O₃F₂ compounds, the contributions from each atom and each state were further investigated using the SHG density method and band-resolved SHG response analysis (with the results shown in Figs. 5 and 6). As described elsewhere, 63 total SHG response derives from virtual-electron (VE) and virtual-hole (VH) processes. The contributions of the VE process to the SHG response of $AB_2O_3F_2$ (A = Ba, Sn, Pb) were shown from the obtained results to be 75.9%, 154.0%, and 51.4%, respectively. Here, we discuss the main contribution of $AB_2O_3F_2$ (A = Ba, Sn, Pb) compounds to the SHG density. Figures 5(a) and 5(b) show the SHG densities of the VE processes for BaB₂O₃F₂ and SnB₂O₃F₂, respectively. Due to the VE process providing a contribution nearly equal to that provided by the VH process, Figs. 5(c) and 5(d) show the SHG densities of the VE and VH processes for PbB₂O₃F₂. As shown in Fig. 5(a), the O and F atoms were indicated to play an important role in determining the SHG response of BaB2O3F2. As for SnB₂O₃F₂ and PbB₂O₃F₂, the oxygen atoms and lone-pair cations Sn/Pb were indicated to provide the main contribution to the total SHG response.

The obtained contributions from each band are shown in Fig. 6. As shown in this figure, the states near the Fermi level were determined to provide the main contribution to the total SHG response. For example, the relatively large peak for SnB₂O₃F₂ was found at region I. The SHG response from the states in region I of SnB₂O₃F₂ was found to be stronger than that of PbB₂O₃F₂ (Fig. 6), which may be due to the distribution of lone-pair electrons in region I. However, unlike SnB₂O₃F₂, with its local peak of SHG response mainly in region I, the local SHG response peak for PbB₂O₃F₂ was found in both region I and region II (from -2.5 eV to the Fermi level), with the integral value of the peak in region II stronger than that of the peak in region I. Furthermore, the results showed a negative contribution made by the VH process to the total SHG response of SnB₂O₃F₂, and nearly equal contributions of the VH and VE processes to the total SHG response of PbB₂O₃F₂.

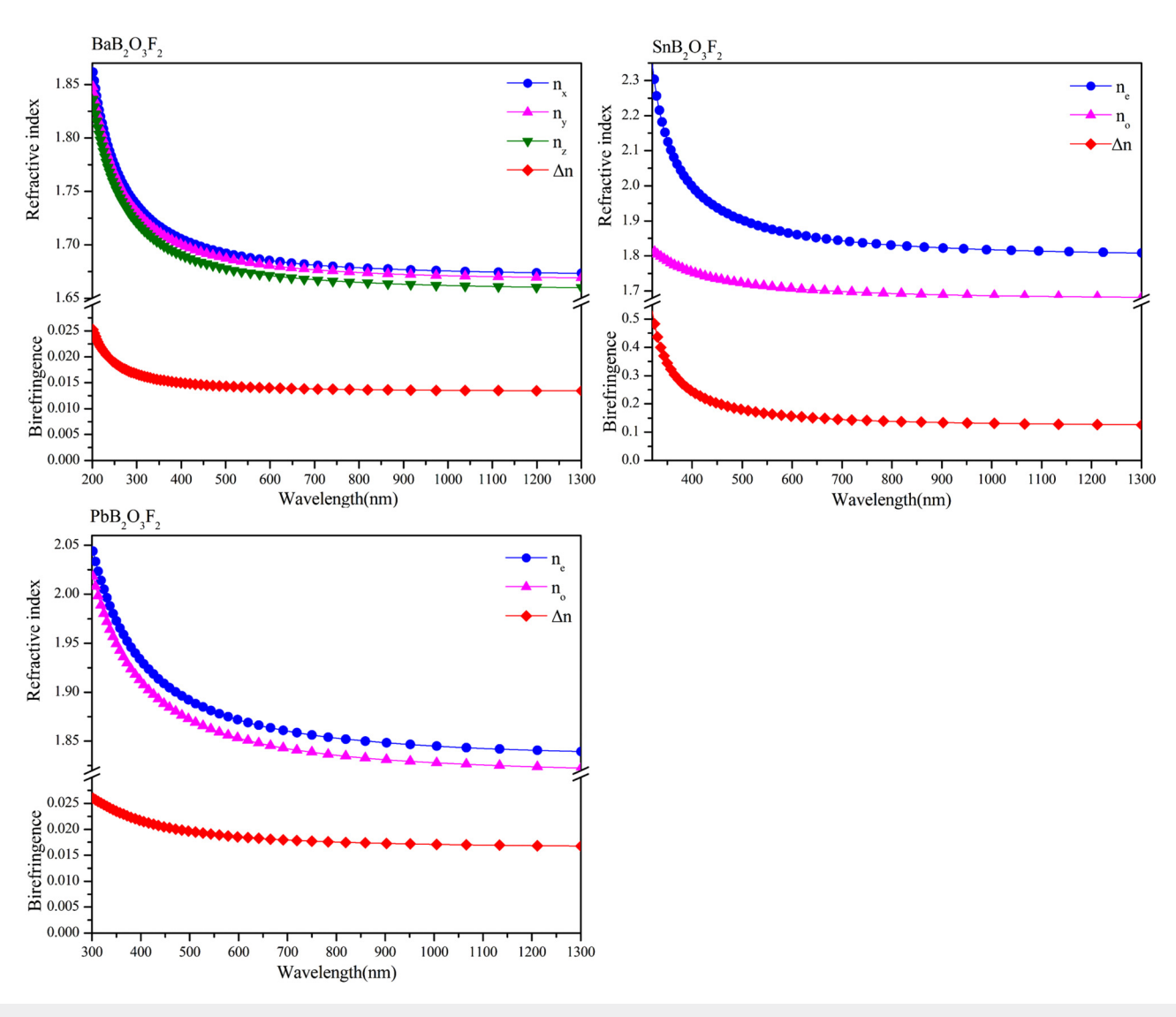


FIG. 4. The refractive indices and birefringence values of AB₂O₃F₂ (A = Ba, Sn, Pb).

The contributions from states in region I and from VH process were concluded to endow the $PbB_2O_3F_2$ compound with a much stronger SHG response than that displayed by $SnB_2O_3F_2$.

A detailed revisit of the results shown in Figs. 1, 2, and 6 is instructive. We paid relatively considerable attention to the states from cations and oxygen atoms, which can help us to form the lone-pair electron distribution. As shown in Figs. 1 and 2, anisotropic lone-pair electron distributions were found at the states in region I (close to Fermi level), while hybrid cation-oxygen states were found in region I and region II. The integral of the peak in region I of $SnB_2O_3F_2$ (1.06) was found to be greater than that of $PbB_2O_3F_2$ (0.18), leading to a larger

lone-pair electron distribution for $SnB_2O_3F_2$ than for $PbB_2O_3F_2$ and hence endowing $SnB_2O_3F_2$ with a relatively strong birefringence due to the relationship between the anisotropic refractive index and the anisotropic electron distribution. The SHG response showed a more complicated relationship with the states near the Fermi level, not only the lone-pair electron distribution found in region I, but also the hybrid cation-oxygen states in region I and region II (even in the low-energy region, such as the states shown in Fig. 6). For the $PbB_2O_3F_2$ compound, more hybrid states were indicated to contribute to the total SHG response, hence endowing it with an SHG response stronger than that of $SnB_2O_3F_2$.

TABLE II. The obtained refractive indices and birefringence values for $AB_2O_3F_2$ (A = Ba, Sn, Pb).

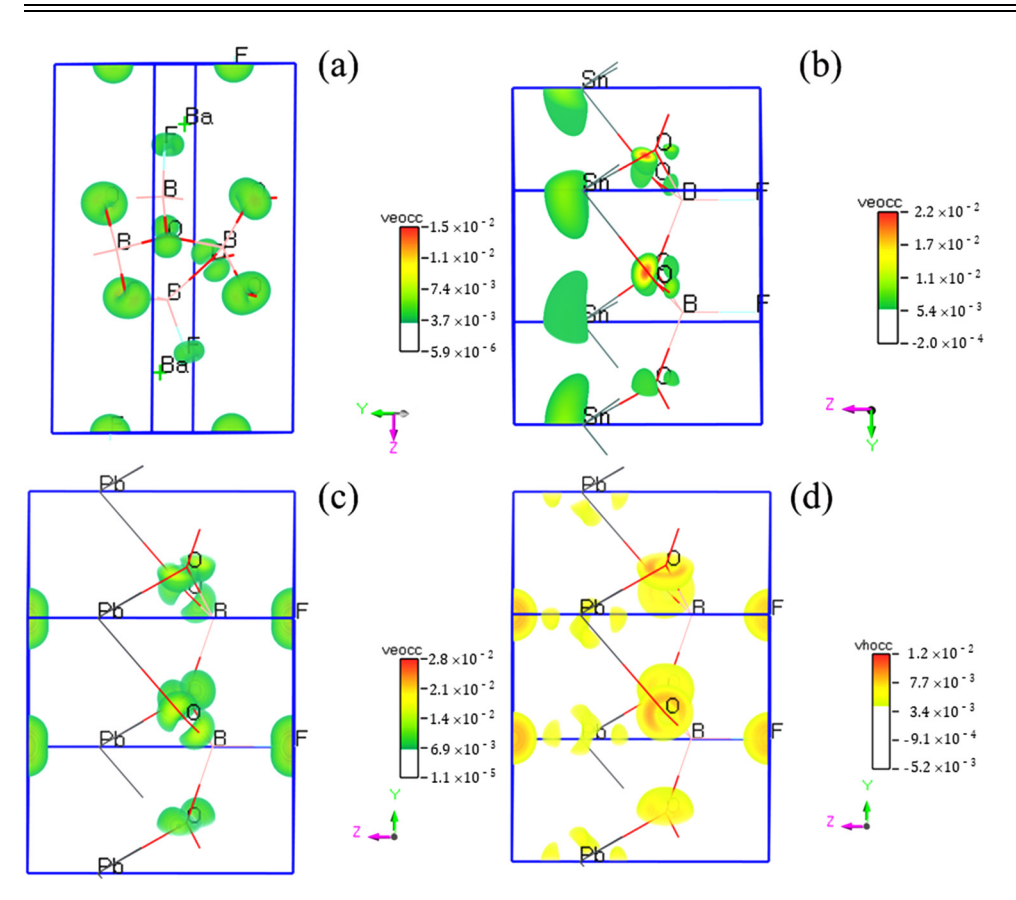
Compound		n_x	n _y	n_z	Δn
$BaB_2O_3F_2$	Origin	1.675	1.670	1.661	0.014
	BOF	1.499	1.493	1.488	0.011
	Ba	1.264	1.261	1.254	0.010
$SnB_2O_3F_2$		n_e		n_o	Δn
	Origin	1.815	1.685		0.130
	BOF	1.534	1.514		0.020
	SnO	1.691	1.514		0.177
$PbB_2O_3F_2$		n_e		n_o	Δn
	Origin	1.843	1.826		0.017
	BOF	1.545	1.545		0.000
	PbO	1.699	1.682		0.017
	PbF	1.581	1.553		0.028

TABLE III. The calculated SHG tensors and powder SHG measurement values of $AB_2O_3F_2$ (A = Ba, Sn, Pb).

Crystal	Calculated SHG tensors (pm/V)	Calculated effective SHG response (pm/V)	Powder SHG measurement values
BaB ₂ O ₃ F ₂	$d_{16} = -0.348;$ $d_{22} = 0.922;$ $d_{23} = -0.387;$ $d_{14} = -0.019$	0.45 (1.4 × KDP)	
$SnB_2O_3F_2$	$d_{15} = -0.037;$ $d_{22} = 0.962;$ $d_{33} = -0.693$	0.73 (2.2 × KDP)	$4 \times \text{KDP}$
PbB ₂ O ₃ F ₂	$d_{15} = -2.712;$ $d_{22} = -2.796;$ $d_{33} = -4.922$	4.30 (13.0 × KDP)	13 × KDP

TABLE IV. The obtained SHG coefficients of $AB_2O_3F_2$ (A = Ba, Sn, Pb).

	d ₁₆	d ₂₂	d ₂₃	d_{14}		d ₁₅	d_{22}	d ₃₃		d_{15}	d_{22}	d ₃₃
Origin	-0.348	0.922	-0.387	-0.019	Origin	-0.037	0.962	-0.693	Origin	-2.712	-2.796	-4.922
BOF	-0.333	0.666	-0.389	0.044	BOF	-0.039	0.122	-1.890	BOF	-0.035	-0.578	-2.664
Ba	0.002	0.112	0.028	-0.023	SnO	-0.101	0.765	0.296	PbO	-3.259	-2.091	-4.375
									PbF	-0.425	-1.044	-1.315



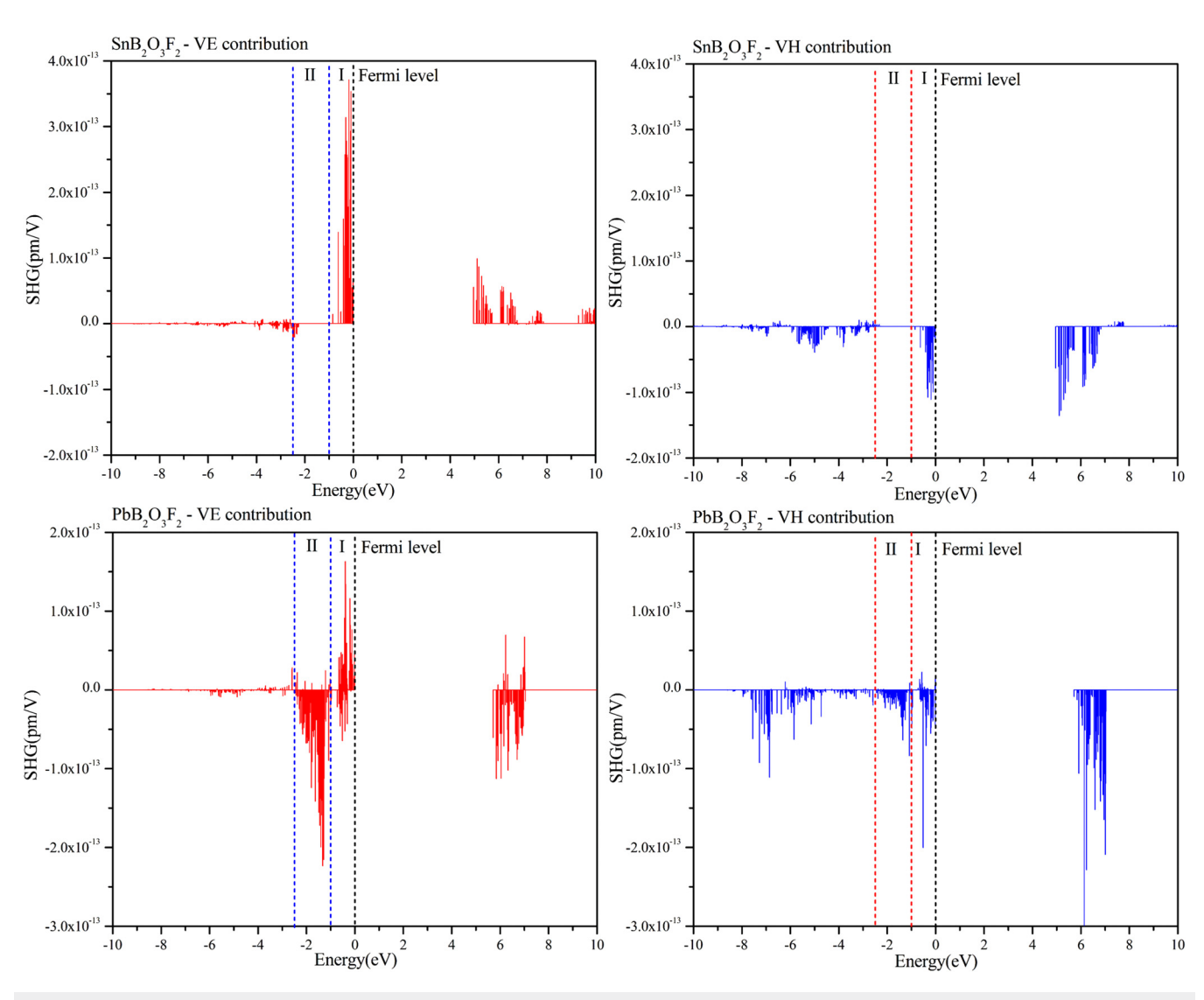


FIG. 6. The band contributions to the total SHG responses of SnB₂O₃F₂ (top) and PbB₂O₃F₂ (bottom).

IV. CONCLUSIONS

In summary, the electronic structures and optical properties of $AB_2O_3F_2$ (A=Ba, Sn, Pb) were investigated using the first-principles method. The results showed anisotropic lone-pair electron distributions in $AB_2O_3F_2$ (A=Sn, Pb) in the states, particularly hybrid cation sp-oxygen p states, near the Fermi level. The lone-pair electron distribution of $SnB_2O_3F_2$ was calculated to be stronger than that of $PbB_2O_3F_2$. The obtained birefringence values of $AB_2O_3F_2$ (A=Ba, Sn, Pb) followed the sequence Sn>Pb>Ba, while the obtained SHG responses of $AB_2O_3F_2$ (A=Ba, Sn, Pb) followed the sequence Pb>Sn>Ba. The expanded hybrid cation-oxygen states endowed $PbB_2O_3F_2$ with a stronger SHG response than those of the other compounds. The difference between the mechanisms for

birefringence and SHG response is expected to be beneficial for obtaining novel NLO compounds.

SUPPLEMENTARY MATERIAL

See the supplementary material for band structures and the projected densities of states (PDOSs) of $AB_2O_3F_2$ (A = Ba, Sn, Pb) with HSE and PBE functionals, the projected band structures by PBE functional, the detailed analysis about orbital diagrams of $PbB_2O_3F_2$ around the Fermi level, the VE and VH contribution of $BaB_2O_3F_2$ from each band, and the formula of effective SHG coefficient.

ACKNOWLEDGMENTS

This work was supported by the Natural Science Foundation of Xinjiang Uygur Autonomous Region of China (Grant No. 2018D01C072).

DATE AVAILABILITY

The data that support the findings of this study are available from the corresponding author upon reasonable request.

REFERENCES

- ¹S.-P. Guo, X. Cheng, Z.-D. Sun, Y. Chi, B.-W. Liu, X.-M. Jiang, S.-F. Li, H.-G. Xue, S. Deng, V. Duppel, J. Kohler, and G.-C. Guo, "Large second harmonic generation (SHG) effect and high laser-induced damage threshold (LIDT) observed coexisting in gallium selenide," Angew. Chem. Int. Ed. 58(24), 8087-8091 (2019).
- ²L. H. Nicholls, F. J. Rodríguez-Fortuño, M. E. Nasir, R. M. Córdova-Castro, N. Olivier, G. A. Wurtz, and A. V. Zayats, "Ultrafast synthesis and switching of light polarization in nonlinear anisotropic metamaterials," Nat. Photonics **11**(10), 628-633 (2017).
- ³A. Tagaya, H. Ohkita, M. Mukoh, R. Sakaguchi, and Y. Koike, "Compensation of the birefringence of a polymer by a birefringent crystal," Science 301(5634), 812-814 (2003).
- ⁴B. Zhang, E. Tikhonov, C. Xie, Z. Yang, and S. Pan, "Prediction of fluorooxoborates with colossal second harmonic generation (SHG) coefficients and extremely wide band gaps: Towards modulating properties by tuning the BO₃/BO₃F ratio in layers," Angew. Chem. Int. Ed. 58(34), 11726-11730 (2019).
- ⁵H. Wu, H. Yu, Z. Yang, X. Hou, X. Su, S. Pan, K. R. Poeppelmeier, and J. M. Rondinelli, "Designing a deep-ultraviolet nonlinear optical material with a large second harmonic generation response," J. Am. Chem. Soc. 135(11), 4215-4218 (2013).
- ⁶Y. Wang, B. Zhang, Z. Yang, and S. Pan, "Cation-tuned synthesis of fluorooxoborates: Towards optimal deep-ultraviolet nonlinear optical materials," Angew. Chem. Int. Ed. 57(8), 2150-2154 (2018).
- ⁷Z. Yang, A. Tudi, B.-H. Lei, and S. Pan, "Enhanced nonlinear optical functionality in birefringence and refractive index dispersion of the deep-ultraviolet fluorooxoborates," Sci. Chin. Mater. 63(8), 1480-1488 (2020).
- ⁸C. T. Chen, T. Sasaki, R. K. Li, Y. C. Wu, Z. S. Lin, Y. Mori, Z. G. Hu, J. Y. Wang, S. Uda, M. Yoshimura, and Y. Kaneda, Nonlinear Optical Borate Crystals, Principles and Applications (John Wiley & Sons, 2012).
- ⁹C. Chen, Y. Wu, and R. Li, "The anionic group theory of the non-linear optical effect and its applications in the development of new high-quality NLO crystals in the borate series," Int. Rev. Phys. Chem. 8(1), 65-91 (1989).
- 10Y. Liu, X. Liu, S. Liu, Q. Ding, Y. Li, L. Li, S. Zhao, Z. Lin, J. Luo, and M. Hong, "An unprecedented antimony(III) borate with strong linear and nonlinear optical responses," Angew. Chem. Int. Ed. 59(20), 7793-7796 (2020).
- 11 B. Zhang, G. Shi, Z. Yang, F. Zhang, and S. Pan, "Fluorooxoborates: Beryllium-free deep-ultraviolet nonlinear optical materials without lavered growth," Angew. Chem. Int. Ed. **56**(14), 3916–3919 (2017).

 12H. Wu, S. Pan, K. R. Poeppelmeier, H. Li, D. Jia, Z. Chen, X. Fan, Y. Yang,
- J. M. Rondinelli, and H. Luo, "K3B6O10Cl: A new structure analogous to perovskite with a large second harmonic generation response and deep UV absorption edge," J. Am. Chem. Soc. 133(20), 7786-7790 (2011).
- 13G. Shi, Y. Wang, F. Zhan, B. Zhang, Z. Yang, X. Hou, S. Pan, and K. R. Poeppelmeier, "Finding the next deep-ultraviolet nonlinear optical material: NH₄B₄O₆F," J. Am. Chem. Soc. 139(31), 10645–10648 (2017).
- ¹⁴X. Wang, Y. Wang, B. Zhang, F. Zhang, Z. Yang, and S. Pan, "CsB₄O₆F: A congruent-melting deep-ultraviolet nonlinear optical material by combining superior functional units," Angew. Chem. Int. Ed. 56(45), 14119–14123 (2017).

 15 M. Mutailipu, M. Zhang, B. Zhang, L. Wang, Z. Yang, X. Zhou, and S. Pan,
- "SrB₅O₇F₃ functionalized with [B₅O₉F₃]⁶ chromophores: Accelerating the

- rational design of deep-ultraviolet nonlinear optical materials," Angew. Chem. Int. Ed. 57(21), 6095-6099 (2018).
- 16 Z. Zhang, Y. Wang, B. Zhang, Z. Yang, and S. Pan, "Polar fluorooxoborate, NaB₄O₆F: A promising material for ionic conduction and nonlinear optics," Angew. Chem. Int. Ed. 57(22), 6577-6581 (2018).
- 17 H. Huang, C. Chen, X. Wang, Y. Zhu, G. Wang, X. Zhang, L. Wang, and J. Yao, "Ultraviolet nonlinear optical crystal: CsBe₂BO₃F₂," J. Opt. Soc. Am. B 28(9), 2186-2190 (2011).
- 18C. T. Chen, G. L. Wang, X. Y. Wang, and Z. Y. Xu, "Deep-UV nonlinear optical crystal KBe₂BO₃F₂-discovery, growth, optical properties and applications," Appl. Phys. B 97(1), 9-25 (2009).
- 19 C. Chen, Z. Xu, D. Deng, J. Zhang, G. K. L. Wong, B. Wu, N. Ye, and D. Tang, "The vacuum ultraviolet phase-matching characteristics of nonlinear optical KBe₂BO₃F₂ crystal," Appl. Phys. Lett. **68**(21), 2930–2932 (1996). **20**C. Chen, Y. Wang, B. Wu, K. Wu, W. Zeng, and L. Yu, "Design and synthesis
- of an ultraviolet-transparent nonlinear optical crystal Sr₂Be₂B₂O₇," Nature 373(6512), 322-324 (1995).
- ²¹C. Chen, Y. Wu, A. Jiang, B. Wu, G. You, R. Li, and S. Lin, "New nonlinearoptical crystal: LiB₃O₅," J. Opt. Soc. Am. B 6(4), 616-621 (1989).
- ²²Y. Wu, T. Sasaki, S. Nakai, A. Yokotani, H. Tang, and C. Chen, "CsB₃O₅: A new nonlinear optical crystal," Appl. Phys. Lett. 62(21), 2614-2615 (1993).
- 23 P. S. Halasyamani, "Asymmetric cation coordination in oxide materials: Influence of lone-pair cations on the intra-octahedral distortion in d⁰ transition metals," Chem. Mater. 16(19), 3586-3592 (2004).
- ²⁴C. C. Stoumpos, L. Frazer, D. J. Clark, Y. S. Kim, S. H. Rhim, A. J. Freeman, J. B. Ketterson, J. I. Jang, and M. G. Kanatzidis, "Hybrid germanium iodide perovskite semiconductors: Active lone pairs, structural distortions, direct and indirect energy gaps, and strong nonlinear optical properties," J. Am. Chem. Soc. 137(21), 6804-6819 (2015).
- 25X. Chen, H. Jo, and K. M. Ok, "Lead mixed oxyhalides satisfying all fundamental requirements for high-performance mid-infrared nonlinear optical materials," Angew. Chem. Int. Ed. 59(19), 7514-7520 (2020).
- 26 K. M. Ok, "Functional layered materials with heavy metal lone pair cations, Pb²⁺, Bi³⁺, and Te⁴⁺," Chem. Commun. **55**(85), 12737–12748 (2019).
- ${\bf ^{27}}Z.$ Chen, S. Pan, Z. Yang, X. Dong, X. Su, and Y. Yang, "Pb $_2B_5O_9Cl:$ A chloride borate with second harmonic generation effect," J. Mater. Sci. 48(6), 2590-2596 (2013).
- 28 E. L. Belokoneva, Y. K. Kabalov, O. V. Dimitrova, and S. Y. Stefanovich, "New hilgardite-group polyborate Pb2[B5O9]Br with high optical nonlinearity," Crystallogr. Rep. 48(1), 44-48 (2003).
- 29Y.-Z. Huang, L.-M. Wu, X.-T. Wu, L.-H. Li, L. Chen, and Y.-F. Zhang, "Pb2B5O9I: An iodide borate with strong second harmonic generation," J. Am. Chem. Soc. 132(37), 12788-12789 (2010).
- **30**G. Zou, C. Lin, H. Jo, G. Nam, T.-S. You, and K. M. Ok, "Pb₂BO₃Cl: A tailormade polar lead borate chloride with very strong second harmonic generation," Angew. Chem. Int. Ed. 55(39), 12078-12082 (2016).
- 31 M. Luo, Y. Song, F. Liang, N. Ye, and Z. Lin, "Pb2BO3Br: A novel nonlinear optical lead borate bromine with a KBBF-type structure exhibiting strong nonlinear optical response," Inorg. Chem. Front. 5(4), 916-921 (2018).
- 32H. Yu, N. Z. Koocher, J. M. Rondinelli, and P. S. Halasyamani, "Pb₂BO₃I: A borate iodide with the largest second-harmonic generation (SHG) response in the KBe2BO3F2 (KBBF) family of nonlinear optical (NLO) materials," Angew. Chem. Int. Ed. 57(21), 6100-6103 (2018).
- 33X. Dong, Q. Jing, Y. Shi, Z. Yang, S. Pan, K. R. Poeppelmeier, J. Young, and J. M. Rondinelli, "Pb2Ba3(BO3)3Cl: A material with large SHG enhancement activated by Pb-chelated BO3 groups," J. Am. Chem. Soc. 137(29), 9417-9422
- 34Q. Jing, X. Dong, Z. Yang, and S. Pan, "Synthesis and optical properties of the first lead borate bromide with isolated BO3 groups: Pb2Ba3(BO3)3Br," Dalton Trans. 44(38), 16818-16823 (2015).
- 35H. Hellwig, J. Liebertz, and L. Bohatý, "Exceptional large nonlinear optical coefficients in the monoclinic bismuth borate BiB₃O₆ (BIBO)," Solid State Commun. 109(4), 249-251 (1998).

- 36 Z. Lin, Z. Wang, C. Chen, and M.-H. Lee, "Mechanism for linear and nonlinear optical effects in monoclinic bismuth borate (BiB₃O₆) crystal," J. Appl. Phys. 90(11), 5585-5590 (2001).
- ³⁷W.-L. Zhang, W.-D. Cheng, H. Zhang, L. Geng, C.-S. Lin, and Z.-Z. He, "A strong second-harmonic generation material Cd₄BiO(BO₃)₃ originating from 3chromophore asymmetric structures," J. Am. Chem. Soc. 132(5), 1508-1509
- 38_{S. Liu, X. Liu, S. Zhao, Y. Liu, L. Li, Q. Ding, Y. Li, Z. Lin, J. Luo, and} M. Hong, "An exceptional peroxide birefringent material resulting from d-π interactions," Angew. Chem. Int. Ed. 59(24), 9414-9417 (2020).
- 39J. Guo, A. Tudi, S. Han, Z. Yang, and S. Pan, "Sn₂B₅O₉Cl: A material with large birefringence enhancement activated via alkaline-earth metal substitution by tin," Angew. Chem. Int. Ed. 58(49), 17675-17678 (2019).
- 40M. Luo, F. Liang, Y. Song, D. Zhao, N. Ye, and Z. Lin, "Rational design of the first lead/tin fluorooxoborates MB2O3F2 (M = Pb, Sn), containing flexible twodimensional [B₆O₁₂F₆]∞ single layers with widely divergent second harmonic generation effects, J. Am. Chem. Soc. **140**(22), 6814–6817 (2018).

 41 M. D. Segall, P. J. D. Lindan, M. J. Probert, C. J. Pickard, P. J. Hasnip,
- S. J. Clark, and M. C. Payne, "First-principles simulation: Ideas, illustrations and the CASTEP code," J. Phys. Condens. Matter 14(11), 2717-2744 (2002).
- 42S. J. Clark, M. D. Segall, C. J. Pickard, P. J. Hasnip, M. I. J. Probert, K. Refson, and M. C. Payne, "First principles methods using CASTEP," Zeitschrift Kristallogr. Cryst. Mater. 220(5/6), 567-570 (2005).
- 43A. M. Rappe, K. M. Rabe, E. Kaxiras, and J. D. Joannopoulos, "Optimized pseudopotentials," Phys. Rev. B **41**(2), 1227–1230 (1990).

 44D. R. Hamann, M. Schlüter, and C. Chiang, "Norm-conserving pseudopoten-
- tials," Phys. Rev. Lett. 43(20), 1494-1497 (1979).
- 45 M. Ernzerhof and G. E. Scuseria, "Assessment of the Perdew-Burke-Ernzerhof exchange-correlation functional," J. Chem. Phys. 110(11), 5029-5036
- ⁴⁶J. P. Perdew, K. Burke, and M. Ernzerhof, "Generalized gradient approximation made simple," Phys. Rev. Lett. 77(18), 3865-3868 (1996).
- ⁴⁷R. J. Nicholls, A. J. Morris, C. J. Pickard, and J. R. Yates, "OptaDOS—A new tool for EELS calculations," J. Phys. Conf. Ser. 371(1), 012062 (2012).
- ⁴⁸A. J. Morris, R. J. Nicholls, C. J. Pickard, and J. R. Yates, "OptaDOS: A tool for obtaining density of states, core-level and optical spectra from electronic structure codes," Comput. Phys. Commun. 185(5), 1477-1485 (2014).
- ⁴⁹J. Lin, M.-H. Lee, Z.-P. Liu, C. Chen, and C. J. Pickard, "Mechanism for linear and nonlinear optical effects in β-BaB₂O₄ crystals," Phys. Rev. B 60(19), 13380-13389 (1999).

- 50B. B. Zhang, M. H. Lee, Z. H. Yang, Q. Jing, S. L. Pan, M. Zhang, H. P. Wu, X. Su, and C. S. Li, "Simulated pressure-induced blue-shift of phase-matching region and nonlinear optical mechanism for K₃B₆O₁₀X (X = Cl, Br)," Appl. Phys. Lett. 106(3), 031906 (2015).
- ⁵¹H. Xiao, J. Tahir-Kheli, and W. A. Goddard, "Accurate bandgaps for semiconductors from density functional theory," J. Phys. Chem. Lett. 2(3), 212-217
- 52M. K. Y. Chan and G. Ceder, "Efficient bandgap prediction for solids," Phys. Rev. Lett. 105(19), 196403 (2010).
- ⁵³J. Heyd and G. E. Scuseria, "Assessment and validation of a screened Coulomb hybrid density functional," J. Phys. Chem. 120(16), 7274-7280 (2004).
- ⁵⁴J. Paier, M. Marsman, K. Hummer, G. Kresse, I. C. Gerber, and J. G. Ángyán, "Erratum: "Screened hybrid density functionals applied to solids,"" J. Chem. Phys. 125(24), 249901 (2006).
- 55 A. V. Krukau, O. A. Vydrov, A. F. Izmaylov, and G. E. Scuseria, "Influence of the exchange screening parameter on the performance of screened hybrid functionals," J. Chem. Phys. 125(22), 224106 (2006).
- ⁵⁶W. Jia, Z. Cao, L. Wang, J. Fu, X. Chi, W. Gao, and L.-W. Wang, "The analysis of a plane wave pseudopotential density functional theory code on a GPU machine," Comput. Phys. Commun. 184(1), 9-18 (2013).
- 57W. Jia, J. Fu, Z. Cao, L. Wang, X. Chi, W. Gao, and L.-W. Wang, "Fast plane wave density functional theory molecular dynamics calculations on multi-GPU machines," J. Comput. Phys. 251, 102-115 (2013).
- $^{\bf 58}$ C. Huang, F. Zhang, H. Li, Z. Yang, H. Yu, and S. Pan, "BaB2O3F2: A barium fluorooxoborate with a unique 2 infinity $[B_2O_3F]^{\text{-}}$ layer and short cutoff edge," Chem. A Eur. J. 25(27), 6693-6697 (2019).
- 59 A. Walsh, D. J. Payne, R. G. Egdell, and G. W. Watson, "Stereochemistry of post-transition metal oxides: Revision of the classical lone pair model,' Chem. Soc. Rev. 40(9), 4455-4463 (2011).
- 60X. Cheng, M.-H. Whangbo, G.-C. Guo, M. Hong, and S. Deng, "The large second-harmonic generation of LiCs₂PO₄ is caused by the metal-cation-centered groups," Angew. Chem. Int. Ed. 57(15), 3933-3937 (2018).
- 61 S. K. Kurtz and T. T. Perry, "A powder technique for the evaluation of nonlinear optical materials," J. Appl. Phys. 39(8), 3798-3813 (1968).
- 62S. J. Cyvin, J. E. Rauch, and J. C. Decius, "Theory of hyper-Raman effects (nonlinear inelastic light scattering): Selection rules and depolarization ratios for the second-order polarizability," J. Chem. Phys. 43(11), 4083-4095
- $^{\bf 63}{\rm C.}$ Aversa and J. E. Sipe, "Nonlinear optical susceptibilities of semiconductors: Results with a length-gauge analysis," Phys. Rev. B 52(20), 14636-14645 (1995).